Suppressing dissolution of vanadium from cation-disordered $Li_{2-x}VO_2F$ via a concentrated electrolyte approach

Musa Ali Cambaz[1], Bhaghavathi P. Vinayan[1], Holger Geßwein[2], Alexander Schiele[3], XXXX, Maximilian Fichtner*[1,3]

[1]Helmholtz Institute Ulm (HIU) Electrochemical Energy Storage, Helmholtzstr. 11, D-89081 Ulm, Germany

[2]Institute for Applied Materials, Karlsruhe Institute of Technology, Herrmann-von-Helmholtz-Platz 1, D-76344 Eggenstein-Leopoldshafen, Germany

[3]Institute of Nanotechnology, Karlsruhe Institute of Technology, D-76344 Eggenstein-Leopoldshafen, Germany

[4]Institute of Surface Chemistry and Catalysis, Ulm University, Albert-Einstein-Allee 47, D-89081 Ulm, Germany

E-Mail: m.fichtner@kit.edu

Keywords: *cation-disordered, rock salt oxides, cathode, lithium-ion battery*

Abstract:

Li_2VO_2F with the cation-disordered rock-salt structure is an attractive high-energy density positive electrode material, but suffers from severe capacity fading upon cycling. The underlying reasons are yet unclear. In this study, we can associate the critical relation of the capacity fade with the electrode-electrolyte interactions such as vanadium dissolution and interfacial resistance build-up upon cycling. In this regard, the use of a concentrated electrolyte, 5.5 M LiFSI in dimethyl carbonate, reduces vanadium dissolution significantly. Moreover, it results in a lower interfacial resistance build-up as compared to conventional 1.0 M $LiPF_6$ electrolyte, thus significantly increasing the cycling stability. We identify that solubility of vanadium enhances significantly with higher oxidation states. Using differential electrochemical mass spectroscopy we demonstrate that oxygen loss does not take place even for highly abusive charging to 4.8 V. Up to now, the ability to drive the full lithiation of VO_2F towards stoichiometric Li_2VO_2F remained, which we are addressing here. This study provides encouraging evidence that electrode-electrolyte interactions have to be considered to improve the cycling performance of vanadium based disordered rock-salt oxides.

Introduction:

Improving the energy density of rechargeable batteries is one of the core objectives in the energy storage field. Debatable, the positive electrode material is the bottleneck to improve the specific energy of the lithium-ion batteries. While an alloying material like Si could offer high specific capacity at the anode side this needs to be balanced with suitable high capacity cathodes. State-of-the art layered rock-salt oxides like $LiCoO_2$ and $LiNi_{1/3}Mn_{1/3}Co_{1/3}O_2$ exhibit stable specific capacities between 145–165 mAh g^{-1}, but practically could not exceed specific capacities higher than 200 mAh g^{-1}.[1–3]This limitation for intercalation based systems stems from the fact that the redox capacity is governed solely by cationic redox of the transition metal, which is either limited by the heavy framework, electronic structure (limited redox stability) or structural stability of the host lattice (cation migration). The development of lithium-rich layered metal oxides based on manganese with $xLi_2MnO_3*(1-x)LiMO_2$ cathodes, is a breakthrough as this material display high capacities in the range between 250-300 mAh g^{-1}, which is by virtue of reversible storage of charge, on both the transition metal and the anion (oxygen redox).[4–7]

With the discovery of disordered rock-salt compounds with facilitated lithium diffusion through lithium excess, this class of compounds have evolved into a potential high capacity cathode material.[8] This finding has opened a new perspective in the paradigmatic search for cathode material showing only minor or no cation mixing. The chemical space for the cathode design, which is traditionally dominated by Ni, Mn and Co based oxides, has been broadened. Today, already a large number of high capacity positive electrode materials with disordered rock-salt structure have been reported.[9–12] The commonly pursued approach comprise the formation of hypothetical solid-solution between an divalent or trivalent transition metal with a high-valent charge compensator. These include Ti^{+4}, [13] Zr^{+4},[14] Sb^{+5},[15] Nb^{+5},[16] Mo^{+6} [10] where the transition

metal is anticipated to be electrochemically inactive. Nevertheless, oxygen redox can partially compensate this penalty by contributing to the overall capacity beyond the transition metal redox capacity. This method exhibits two major disadvantages: one is the high atomic mass, leading to a heavier framework structure and lower specific capacities and second the introduced transition metal offers no redox capacity or is active in an impractical voltage window.

An alternative approach is based on the use of transition metals suitable for multiple electron reactions, such as $V^{+3/+5}$,[17,18] $Cr^{+3/+5}$,[19] $Mo^{+3/+6}$,[20] but these usually have lower average voltages. Attempts to increase the average voltage by introducing an additional transition metal with high voltage redox-couples have shown limited success. An encouraging and unusual development for cation-disordered rock-salts is that the unusual distribution of local cation environments gives rise to high level of bulk fluorination.[21] Contrary to classical ordered systems, where only low degree of fluorine could be substituted, fluorine to oxygen substitution has been shown to increase the operation voltage of these oxyfluoride materials and further reduce the oxidation state of the compound and therefore mitigate oxygen release by maximizing transition metal redox.[22] Substitution of O^{2-} for F^{-} offers an attractive alternative to introduce Li-excess compared to the conventional high-valent doping with heavy redox-inactive elements and therefore offers high theoretical capacities. Although new materials and design concepts have been introduced, long cycling stability with minor capacity fading yet has to be demonstrated. Here, approaches could be promising where the transition metal redox capacity is maximized by employing multi-electron redox couples, in order to avoid oxygen oxidation with irreversible O_2 gas release.

Cubic disordered rock-salt Li_2VO_2F synthesized by a direct mechanochemical approach shows a theoretical capacity of 462 mAh g^{-1} with the feasibility for $V^{+3/+5}$ redox reaction.[18] Its preparation requires a mechanochemical synthesis without heat treatment due to thermal

instability, which rules out classical solid-state synthesis.[23] Alternatively, the isostructural phase can be synthesized by electrochemical lithiation of a rhombohedral VO_2F perovskite phase, leading to an irreversible phase transition and the cubic disordered $Li_{2-x}VO_2F$ end phase.[17,23–25] Li_2VO_2F is an attractive high-energy density positive electrode material, but, according to recent reports, suffers from severe capacity fading upon cycling. The reasons for the capacity fade were still unclear.

In this work, we focus our efforts on the critical aspect of the electrode–electrolyte interaction of $Li_{2-x}VO_2F$. This comprises metal dissolution from the electrode material and an increase in the cell resistance due to the formation of a blocking surface leading to fatigue of the cell. We have used highly concentrated 5.5M LiFSI dimethyl carbonate (DMC) electrolyte, [26,27] and compared it to standard 1M $LiPF_6$ in DMC and ethylene carbonate (EC) electrolyte. There are variety of possible side reactions of positive electrode materials, acid-base interactions with HF and PF_5(strong Lewis acid) are particularly important with regard to metal dissolution, which are inevitably present or were formed with $LiPF_6$ electrolytes.[28] LiFSI as chemically more stable salt compared to conventional $LiPF_6$ promise to alleviate these.[29] Vanadium dissolution from the positive electrode was hinted by our previous work which we quantified for both electrolytes. Vanadium deposition on the anode was observed and analyzed by XPS and Raman spectroscopy. The influence of the electrolyte on the cycling performance of $Li_{2-x}VO_2F$ has been elaborated by electrochemical analysis and impedance spectroscopy. We have also shown the feasibility to lithiate VO_2F with 2 Li per f.u. The charge-compensation mechanism has been elucidated by XANES. DEMS analysis shows that no oxygen is released even for cut-offs >4.7 V *vs* Li^+/Li^0.

Result

I. Synthesis & Characterization

The cation-disordered rock-salt Li_2VO_2F can either be synthesized by a direct mechanochemical approach or through the lithiation of perovskite VO_2F phase. VO_2F can theoretically accommodate up to 2 Li per formula unit, corresponding to a $V^{3+/5+}$ redox reaction.[18,25] This can be realized either electrochemically by discharging the cell with lithium anode as lithium source or chemically by a reducing agent like n-butyllithium. (n-BuLi), which can mimic the electrochemical lithiation. For the electrochemical lithiation to $Li_{2-x}VO_2F$, cells have been constructed and then discharged to 1.3 V versus Li/Li^+ at 20 mA g^{-1} current, exhibiting a discharge capacity of 450 mAh g^{-1} , which corresponds to 1.7 Li per formula unit. For the chemical lithiation, 2.1 equivalents of n-BuLi have been used, which gave a nominal stoichiometry of Li_2VO_2F according to ICP-OES. Details are given in the Supplementary Information (SI). The electrochemically synthesized compounds will be noted as $Li_{2-x}VO_2F$ due to the off-stoichiometry in order to distinguish between both compounds. The synthesis of *R-3c* VO_2F has been adopted from our previous work. The high-resolution transmission electron microscopy (HRTEM) overview is shown in **Figure 1a** and reveals the typical morphology, which is seen for mechanochemically synthesized material.[30,31] The sample consists of larger agglomerated particles composed of smaller grains with intersecting amorphous regions. The crystallites are in the range of around 20-50 nm. **Figure 1a** shows the HRTEM image of VO_2F along the [001] zone. In **Figure 1b** the elements V, O, F have been confirmed by electron energy loss spectroscopy with a vanadium oxidation state of +5. The XRPD pattern of the pristine VO_2F with a rhombohedral structure with space group *R-3c* is presented in **Figure 1c**. The refined lattice parameters are $a = b = 5.134524$ Å, $c = 13.00811$ and V = 296.992 $Å^3$. The XRPD of Li_2VO_2F and $Li_{2-x}VO_2F$ are shown in **Figure 1d,e.** Both compound adopt a cubic disordered rock-salt-type structure with *Fm-3m* space group. The refined lattice parameter for Li_2VO_2F is $a = 4.118305$ Å and for $Li_{2-x}VO_2F$ is $a = 4.11807$ Å. The lattice parameter of both compounds

deviate slightly due to the differences in composition. **Figure 1f** shows the schematic crystal structure of rhombohedral VO_2F and cubic Li_2VO_2F.

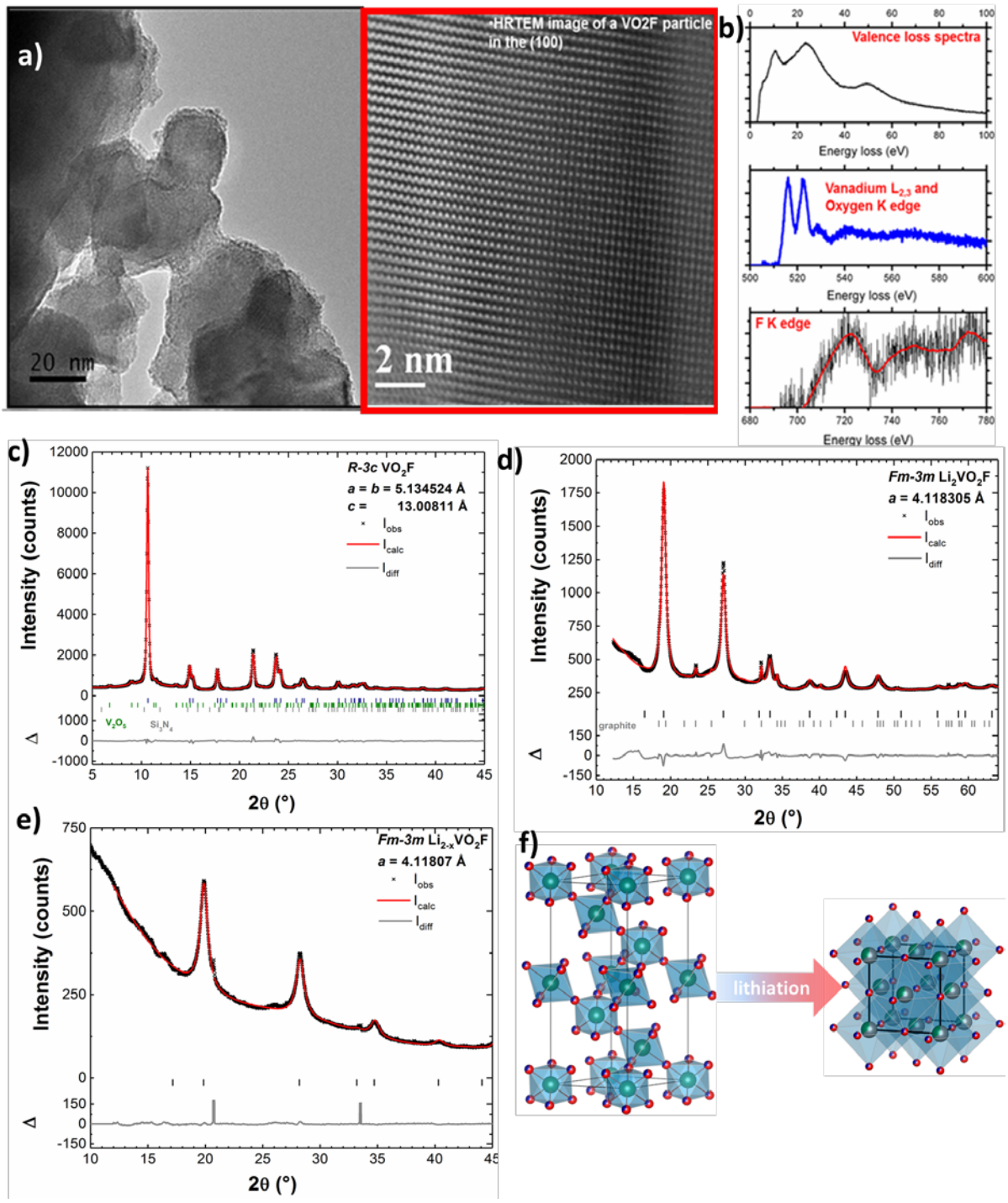

Figure 1: a) HRTEM of VO_2F with an inset along the [001] zone **b)** EELS of VO_2F with valence loss region, vanadium $L_{2,3}$ edge oxygen K-edge and fluorine K-edge **c)** rhombohedral VO_2F (*R-3c*) **d)** cubic $Li_2VO_2F^{\#}$ (*Fm-3m*) **e)** cubic $Li_{2-x}VO_2F$ (*Fm-3m*) f)Schematic illustration of the crystal structures for rhombohedral VO_2F and cubic Li_2VO_2F.[32] $^{\#}Li_2VO_2F$/C composite

Electrochemistry:

We compared the electrochemical properties of Li_2VO_2F and $Li_{2-x}VO_2F$, which were tested in the voltage range of 1.3-4.1 V at 20 mA g^{-1} current. It's important to note that a $2e^-$ transfer corresponds to a specific capacity of 463 mAh g^{-1} for Li_2VO_2F and 526 mAh g^{-1} for VO_2F ($Li_{2-x}VO_2F$) due to the lighter framework. **Figure 2a** with Li_2VO_2F shows a first discharge of 355 mAh g^{-1} (1.53 Li per f.u.) with a plateau like behavior around 2.5 V as shown by the corresponding differential capacity versus voltage curves. **Figure 2b** shows the first discharge of VO_2F capacity of 440 mAh g^{-1} (1.67 Li per f.u.) with a sloping profile for the first cycle. The consecutive cycles resemble the charge-discharge profile of Li_2VO_2F. The first cycle shows a comparably high irreversible capacity, which we observed already in our previous work for the delithiation of rhombohedral Li_xVO_2F.[17] A closer look at the corresponding differential capacity (dQ dV^{-1}) versus V plot show several peaks for the first discharge, but only one peak for the consecutive cycles. This can possibly be attributed to the irreversible rhombohedral to cubic phase transition during the first cycle. For the second cycle both compounds show similar behavior with a plateau-like behavior at 2.5 V indicating the chemical similarity of both compounds. **Figure 2c** shows the cycling stability for different specific currents at 10, 20, 50, 100 mA g^{-1} for $Li_{2-x}VO_2F$ and at 50 mA $g^{-1}$for Li_2VO_2F. $Li_{2-x}VO_2F$ shows for the same specific current a better cycling stability as compared to Li_2VO_2F. It is noteworthy that the capacity retention is lower for slow cycling and increases with the current density. This could hint at a chemical instability of the material when in contact with the electrolyte, as lower rates mean longer contact times. **Figure 2d** shows the cycling stability and the specific current at 100 mAh g^{-1} for various voltage windows. The voltage window limits the governing redox reaction and therefore the amount of inserted/extracted lithium. The voltage window has been varied systematically by fixing either the upper cut-off to 4.1 V or the lower cut-off and gradually

changing window. In this respect, varying the lower cut-off increases the specific discharge capacity due to the sloping profile drastically. In contrast, increasing of the upper cut-off from 4.1 V towards 4.5 V leads to increasing capacity fading. The capacity retention decreases for higher cut-offs (>4.1 V) and slower cycling, which indicates possible side reactions and instabilities of the electrode-electrolyte interface.[33] In a second attempt, a concentrated 5.5 M lithium bis(fluorosulfonyl) imide (LiFSI) in dimethyl carbonate electrolyte[34] was examined and compared to a conventional 1.0 M $LiPF_6$ in ethylene carbonate dimethyl carbonate (1:1 w/w) electrolyte. Hereafter, we will use the notation 5.5M-LiFSI and 1.0M-$LiPF_6$, respectively. The cycling stability has been studied at a specific current of 100 mA g^{-1} in the cycling window between 4.1-1.3 V as shown in **Figure 2e**. Common for both electrolytes is the high first cycle irreversibility. For the cells with 5.5M-LiFSI the cycling stability increased significantly, exhibiting a specific capacity of 155 mAh g^{-1} after 200 cycles compared to the cells with 1.0M-$LiPF_6$ electrolyte exhibiting only 30 mAh g^{-1}. **Figure 2f** illustrates the rate performance with both electrolytes, which involved five consecutive cycles at a constant specific current at 20, 50, 100, 200, 400, 800 mA g^{-1}. The cells with 1.0M-$LiPF_6$ exhibited a capacity of 372, 355, 324,287,231, 143 mAh g^{-1} for the respective 2^{nd} cycle. For 5.5M-LiFSI the corresponding values were 364, 349, 321, 289, 249, 190 mAh g^{-1}. For higher cycle numbers the discharge capacity diverged more due to comparably higher capacity fading of the cells with 1.0M-$LiPF_6$ electrolyte. **Figure 2g,h** shows the charge-discharge profile of the 2^{nd} cycle of each current range from the rate-capability test, respectively.

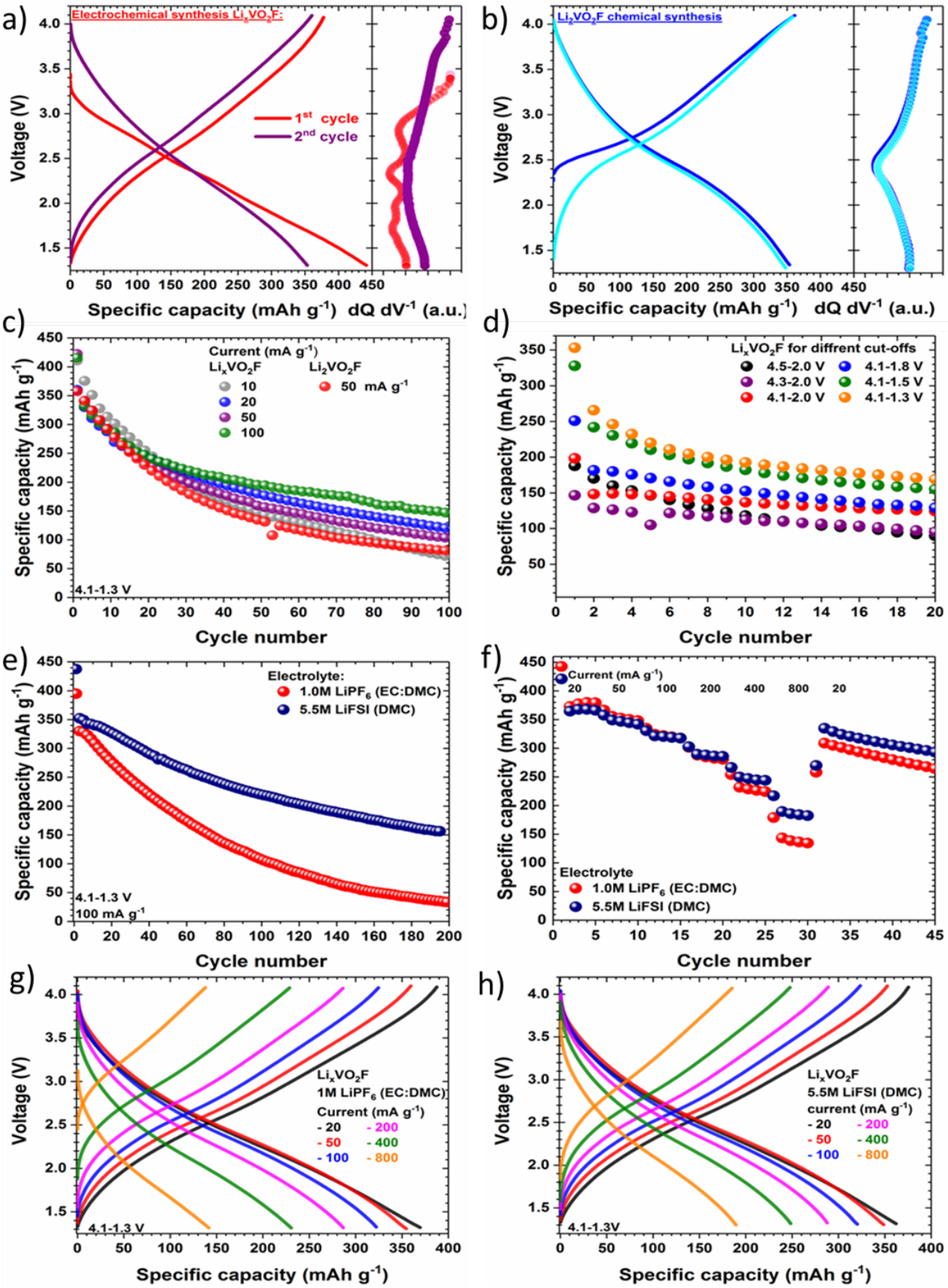

Figure 2: Cycling measurements were conducted in the voltange between 4.1-1.3 V unless stated otherwise. Charge-discharge profile of **a)** Li_2VO_2F **b)** $Li_{2-x}VO_2F$ at 20 mA g^{-1} with

corresponding dQ dV^{-1}.**c)** Cycling stability for various specific currents **d)** Cylcing stability of $Li_{2-x}VO_2F$ for different cut-offs. **e)** Cycling stability of $Li_{2-x}VO_2F$ at 100 mA g^{-1} for 1.0M-$LiPF_6$ and 5.5M-LiFSI. **f)** Rate capacbility test for $Li_{2-x}VO_2F$ for 1.0M-$LiPF_6$ and 5.5M-LiFSI. Respective charge-discharge profile from rate capability test at different specific currents for **g)** 1.0M-$LiPF_6$ **h)** 5.5M-LiFSI.

Degradation mechanism: Electrode-electrolyte interactions

The results highlight the importance of the optimized electrolyte on the cycling stability of $Li_{2-x}VO_2F$. It is in general accepted that all positive electrode materials can react with commonly used electrolytes, which leads to a unique surface chemistry and a possible passivation.[33] To understand the origins of the capacity fade and the influence of the electrolyte on the degradation mechanism complementary investigations were carried out with a focus on the electrode-electrolyte interactions with the positive electrode side.

The lithium anode of an aged cell was investigated by X-ray photoelectron spectroscopy (XPS) and Raman Spectroscopy. XPS was used to probe the oxidation state of the deposited vanadium on the lithium anode surface; the V 2p core level is shown in **figure 3b**. The deconvolution of vanadium gives the $V2p_{3/2}$ peak at 516.1 eV and $V2p_{1/2}$ peak at 523.5 eV, respectively and indicates +4 valence state of vanadium.[35] Furthermore, a surface mapping of vanadium on cycled Li has been done by Raman spectroscopy. It should be noted that Raman spectra are very sensitive to crystal symmetry, coordination geometry and oxidation states, which make the profound analysis difficult. In the current study, we used Raman only to map the vanadium deposits on the lithium anode. **Figure S1** shows the Raman spectra of cycled Li surface and compared with V_2O_5 reference spectra. The spectra illustrate the deposition of an amorphous VO_x -like film on the cycled lithium surface, with the majority of vanadium in V^{+4} oxidation state. This observation is in accordance with the XPS results. **Figure 3a** shows the Raman

mapping of the vanadium on the cycled Li surface using the intensity of vanadium~ 900 cm^{-1} peak, which is the most intense peak and mainly originates due to the stretching vibration of the vanadyl bonds. [36,37]

In order to understand the origins of the performance improvements for $Li_{2-x}VO_2F$, electrochemical impedance spectroscopy (EIS) was performed on cycled cells. Furthermore, the extent of vanadium dissolution was qualitatively probed for both electrolytes. EIS was measured at 25 °C for the discharged state after the first formation and the 50th cycle. The Nyquist plots for the positive electrode with 1.0M-$LiPF_6$ and 5.5M-LiFSI are shown in **Figure 3c,d** respectively. The Nyquist plot shows a semicircle at high frequency region, which can be attributed to the surface film resistance (R_{sf}) and the charge transfer resistance (R_{ct}) as shown in the fitted circuit. R_{sf} originates from the bulk electrode electronic resistivity and electrolyte resistance, R_{ct} is due to the charge transfer resistance at the electrode-electrolyte interface. The sloping line is attributed to the solid-state diffusion of the Li^+-ions in the bulk (Warburg element). R_{sf} resistance for 1.0M-$LiPF_6$ after 2nd cycle and 50th cycle were 1.6 **Ω** and 2.6 **Ω**, respectively. The corresponding R_{sf} values for 5.5M-LiFSI were 8.7 **Ω** and 8.2 **Ω**, respectively. The relatively larger R_{sf} values for 5.5M-LiFSI, could be due to the high viscosity of concentrated electrolyte or as a result of a more dense surface film due to the decomposition of LiFSI salt. The charge transfer resistances R_{ct} for 1.0M-$LiPF_6$ after 2nd cycle and 50th cycle were 12 **Ω** and 39 **Ω**, respectively. The corresponding R_{ct} values for 5.5M-LiFSI were 6.8 **Ω** and 9.4 **Ω**, respectively. Remarkably, unlike the drastical increase of the charge-transfer resistance for the cells using 1.0M -$LiPF_6$ (225% increase), the resistances of the cells using 5.5M-LiFSI (38%) increased only slightly, which indicates the formation of a more conductive and stable cathode electrolyte interphase (CEI) for the latter.

For the dissolution study VO_2F and nominal "$Li_{1.7}VO_2F$" have been immersed in both electrolytes for 7 days at 45°C. Afterwards, the amount of vanadium in the electrolyte was

determined by inductively coupled plasma optical emission spectroscopy (ICP-OES) which is summarized in **Table 2**. This study gives a clear indication for the solubility of the vanadium from the positive electrode in the carbonate electrolytes. The pristine VO_2F shows a ~ 20 times higher solubility compared to the lithiated compound. Striking is the difference of the vanadium solubility between the 5.5 M-LiFSi and 1.0M-$LiPF_6$ electrolyte, clearly indicating a lower solubility of vanadium in the more concentrated electrolyte. Together with the observation that the deposited vanadium was found predominantly in the oxidation state +4 and that dissolution was enhanced for pristine state with the oxidation state +5, we argue that higher oxidized vanadium is more soluble in carbonate electrolytes.

Taken together with the ICP-OES results and the impedance measurements, we can clearly demonstrate that the concentrated LiFSI electrolyte approach was effective in lowering the positive electrode material resistance and in suppressing V dissolution. As consequence, the cycling performance was improved significantly.

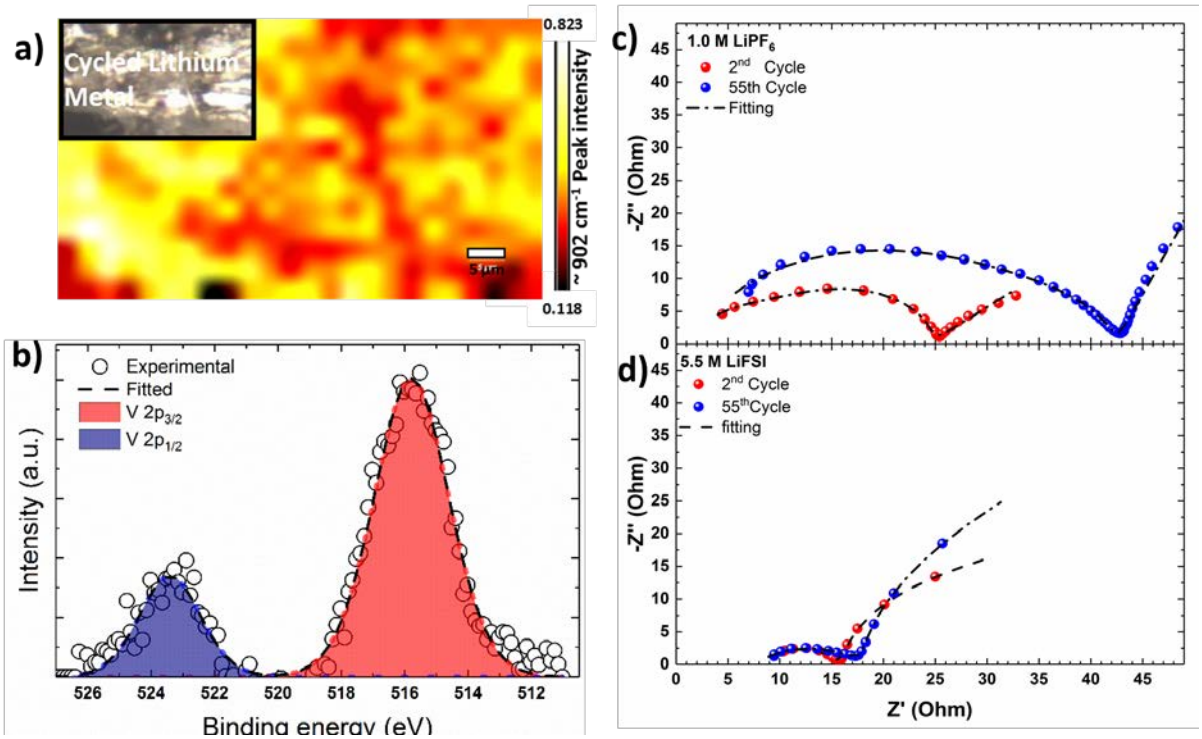

Figure 3: a) Raman mapping of vanadium on the lithium anode **b)** V 2p core level of the vanadium deposited on the anode. EIS measurements on the positive electrode for different cycles **c)** 1.0M-$LiPF_6$ **d)** 5.5M-LiFSI

Table 2: V dissolution in the electrolyte at elevated temperatures (T=45°C) for pristine and discharged state.

Compounds	V dissolution %	
	1.0 M $LiPF_6$	5.5 M LiFSI
VO_2F	4.49±0.13	1.55±0.04
$Li_{1.7}VO_2F$	0.22±0.01	-

Reaction mechanism:

In order to elucidate the charge compensation mechanism for $Li_{2-x}VO_2F$ V K-edge measurements have been performed for different state of charge as shown in **Figure 4a,b** . The comparison of the V K-edge of VO_2F with V_2O_5 reference confirms the oxidation state to be +5 states. VO_2F shows a weak pre-edge located at 5469 eV, which can be attributed to the dipole transition due to p-d hybridization of V in the distorted octahedral environment.[38] Upon discharge (lithiation) from OCV (pristine state) to 1.3 V, the absorption edge shifts to lower energies, close to the value of the reference Li_2VO_2F with +3 oxidation state as shown in **Figure 4a**. This is in accordance with the observed discharge capacity, corresponding to 1.7 Li per f.u. and an oxidation state of ~3.3. Pre-edge peak intensity typically increases with deviation from octahedral symmetry. Moreover, it changes as a function of the number of d-electrons and is maximized for d^0-configuration.[38] The increase of the pre-edge intensity after discharge therefore hints a structural distortion. Upon charging, the V absorption edge shifts to the higher

energy values, but does not recover the edge position of the pristine state with V^{+5} as shown in **Figure 4b**. This observation is in accordance with the first cycle irreversibility.

For lithium-rich materials, both oxygen redox and lattice oxygen loss with cycling are well known phenomena.[39,40] In order to find out whether oxygen release takes place in the case of Li_2VO_2F, *in-situ* differential electrochemical mass spectrometry (DEMS) measurements were conducted. The potential oxygen release was triggered by varying the upper cut-off voltage from 4.5 V in the first cycle to 4.8 V for the second and third cycle. **Figure 4c** compares the potential and the gas evolution profiles for the first three cycles. CO_2 evolution started at 3.6 V, and increased with the potential and can be attributed to electrochemical electrolyte oxidation.[41,42] No oxygen evolution could be detected for the cut-offs 4.5 V and 4.8 V in the consecutive cycles. For the second cycle with the higher cut-off CO evolution was observed at 4.7 V, which possibly can be attributed to the oxidation of conductive carbon.[43]

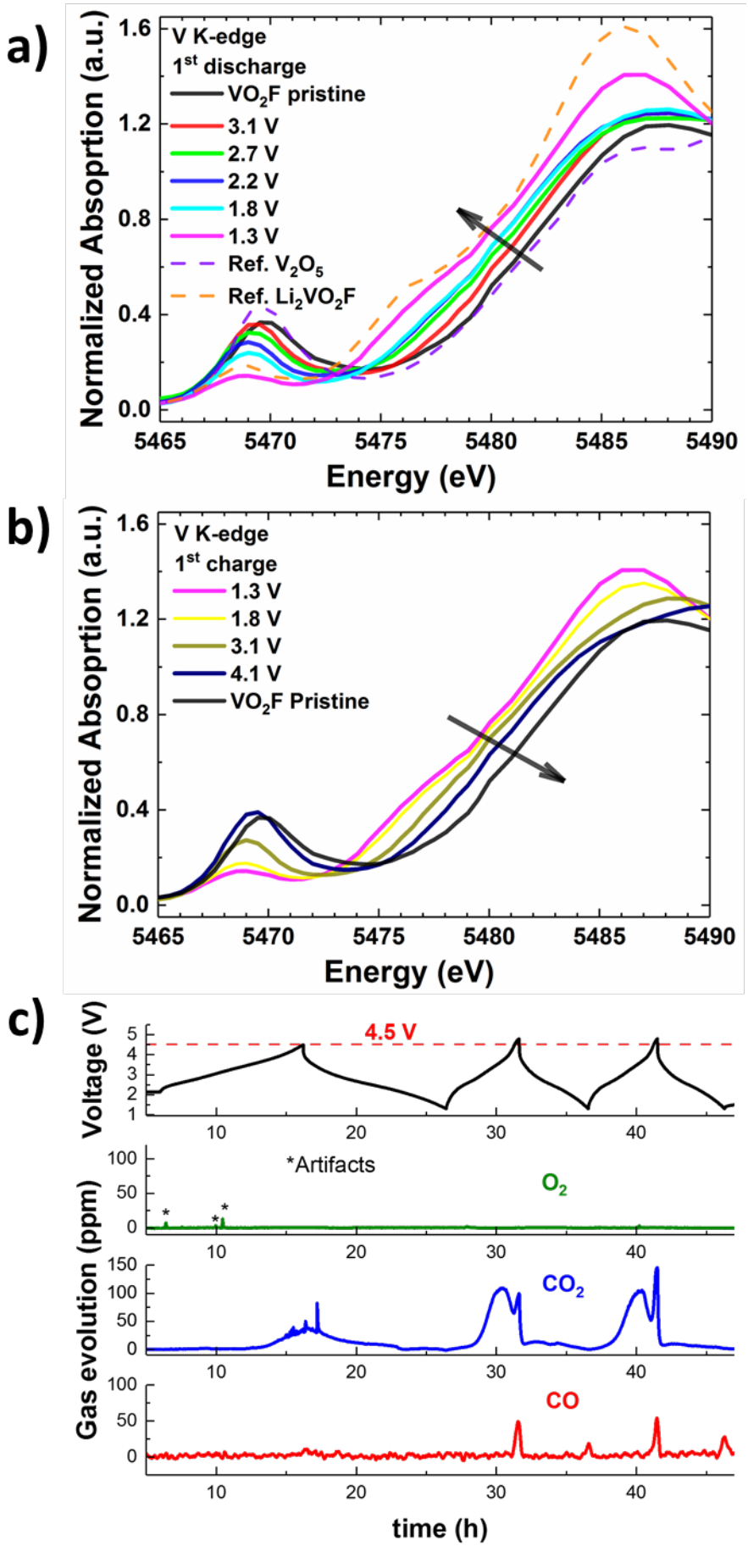
a)
V K-edge
1st discharge
VO2F pristine
3.1 V
2.7 V
2.2 V
1.8 V
1.3 V
Ref. V2O5
Ref. Li2VO2F
Normalized Absoprtion (a.u.)
Energy (eV)
b)
V K-edge
1st charge
1.3 V
1.8 V
3.1 V
4.1 V
VO2F Pristine
Normalized Absoprtion (a.u.)
Energy (eV)
c)
4.5 V
Voltage (V)
*Artifacts
O2
CO2
CO
Gas evolution (ppm)
time (h)

Figure 3:**a)** V K-edge for $Li_{2-x}VO_2F$ for the first discharge from OCV to 1.3 V **b)** V K-edge for the first charge **c)** DEMS measurements of Li_2VO_2F the first charge cycle at C/10 to 4.5 V and to 4.8V for second and third cycle. The cell voltage (black) is shown together with the O_2 (blue) CO_2 (blue) and CO (red) evolution.

Discussion:

Electrode-electrolyte interactions in concentrated electrolyte

Li_2VO_2F is well known to have a severe capacity fading issue, similar to other Li-rich cation-disordered rock-salt oxides. The underlying reasons for these observations are still not completely clarified. In general, surface side reaction with electrolyte, metal dissolution, surface phase evolution due to transition metal migration and oxygen oxidation with irreversible O_2 gas release have been linked to the degradation with these type of materials.[44–46]

In general, two key factors can contribute to the improved cycling stability of $Li_{2-x}VO_2F$ in the high concentrated LiFSI-DMC electrolyte. One is the selection of the electrolyte salt. LiFSI shows higher ionic conductivities in electrolytes due to the weaker interaction between solvated Li^+ cations and the FSI anion as compared to $LiPF_6$ salt and comparably higher Li transference number.[29,47] Another factor is the molecular structure of the electrolyte solution. To understand the differences in the performance the 1M-$LiPF_6$ and highly concentrated electrolyte 5.5M-LiFSI, the molar ratios of solvent and salt have to be considered. The molar ratio of solvent to salt corresponds to 13.6:1 for 1M-LiPF6 and 2.7:1 for 5.5M-LiFSI, which gives rise to an different coordination and solvation of the ions. For the concentrated electrolyte, the ions were mostly contact ion pairs and aggregate solvate clusters, which can explain the relatively higher viscosity and can lead to a decrease in the ionic conductivity.[26,48] Surprisingly, our results show comparable rate capabilities for both electrolytes, which can principally be attributed to the

improved electrolyte stability in terms of reduced solvent (unsolvated) availability and possible sacrificial anion reduction, which is hypothesized to lead to lowered interfacial resistances.

On the basis of our data we can show that capacity fading of $Li_{2-x}VO_2F$ can be alleviated with a concentrated electrolyte by tuning the electrode-electrolyte interactions. We could qualitatively demonstrate that vanadium dissolution of the positive electrode material could effectively be reduced changing from a 1.0 M $LiPF_6$ EC/DMC electrolyte to a concentrated 5.5 M LiFSI DMC electrolyte. Interestingly, we found that dissolution is drastically higher for the charged state as compared to discharged state. The values were derived at elevated temperatures and higher active material to electrolyte ratio, which can increase dissolution, but qualitatively gives the right trend. An AC impedance study on cycled electrodes demonstrated that the charge-transfer resistance increase for the positive electrode material was considerably smaller for the concentrated 5.5M LiFSI electrolyte. The low charge-transfer resistance could be due to the formation of more conductive and stable CEI layer at the electrode-electrolyte interface. Furthermore, we argue that in the case of the concentrated electrolyte, dissolution and migration of transition metal can be suppressed due to the lower quantity of unsolvated solvent molecules. The use of concentrated electrolyte with LiFSI can therefore increase cycle life of $Li_{2-x}VO_2F$. Raman mapping and XPS of the lithium metal anode showed that the vanadium species found on the lithium anode has a mixed oxidation state between +5 and +4, which is unexpected since reduction to metallic form can be anticipated.

Li-rich cation-disordered rock-salt vanadium oxyfluoride:

When we first reported the rhombohedral VO_2F we assumed that the formation of cation-disordered cubic Li_2VO_2F by lithiation could be possible due to the feasibility of $V^{3+/5+}$ redox couple. In the literature, the electrochemical lithiation up to 1.75 Li per f.u.[25] has been reported

for the first discharge, similarly to our finding of 1.7 Li per f.u. Hence, the question about the ability to reach full lithiation remained. We could now show the accessibility up to 2 Li per f.u. is possible by chemical lithiation with the reducing agent nBuLi (~1.0 V *vs* Li^+/Li^0)[49] without indication of amorphization or phase decomposition. Consistent with the first cycle irreversibility, V oxidation is not completely reversible in a moderate cycling window of 4.1-1.3 V. Up to now, the possibility of oxygen release has not been considered even though it has frequently been observed for Li-rich disordered rock-salt materials. To investigate, whether oxygen loss can be triggered we performed DEMS measurements with highly abusive charge-discharge cycles up to 4.7 V without detection of oxygen gas formation. CO_2 formation was observed, however. To the best of knowledge, no oxygen redox activity could be experimentally demonstrated for any vanadium based rock-salt oxides, rather multi-redox processes coupled with vanadium migration has been observed, which has been associated with the peculiar redox chemistry of vanadium based systems.[50] Fluorine incorporation has been regarded as an efficient way to introduce lithium excess in order to achieve lithium percolation and increase transition metal capacity by lowering the oxidation state as in the case of Li_2VO_3/Li_2VO_2F.[51] Recently, the observation with the first cycle irreversibility in cation-disordered oxyfluorides systems have been rationalized by DFT, which predicts the lithium migration in tetrahedral sites for high state of charge. [12,52] Thereby, the strong affinity of Li towards fluorine and necessitates higher extraction voltages, which can cross the electrolyte stability limit.

Conclusion:

In conclusion, we have exploited the capacity fading for the $Li_{2-x}VO_2F$ from the perspective of the electrode-electrolyte interactions. We could significantly improve the cycling stability of this system by using a concentrated electrolyte with 5.5M LiFSI in DMC. We qualitatively demonstrated that vanadium dissolution is a critical issue and that transition metal dissolution reduced in the concentrated electrolytes. In particular, the lowered vanadium solubility and the

reduced interfacial resistances were found to increase the cycling stability. Yet, the cycling stability continuously decreases and hints towards other degradation mechanism. Our study shows that oxygen gas release is unlikely for this system. Furthermore, we demonstrated the feasibility to form Li_2VO_2F by chemical lithiation with n-BuLi. The results presented here provided a novel constraint and suggests opportunities to improve the performance by optimization of the electrode-electrolyte interactions.

Acknowledgements

Financial support by the FET-OPEN project "LiRichFCC" of the European Commission (grant agreement # 711792) is gratefully acknowledged. This work contributes to the research performed at CELEST (Center for Electrochemical Energy Storage Ulm-Karlsruhe.

Experimental Section

Synthesis:

VO_2F: The synthesis procedure was adapted from our previous work.[17] Stoichiometric amounts of V_2O_5 and VOF_3 were ball milled with 600 rpm for 20h using a Fritsch P6 planetary ball mill with an 80 mL silicon nitride vial and silicon nitride ball with an ball to powder ratio of 15:1.

Li_2VO_2F: chemical lithiation was carried out in a Schlenk Tube under argon atmosphere in a freezing bath of dry ice/acetone mixture (-78°C). To a suspension of VO_2F in dry hexane 2.1 equivalents of n-butyllithium (2.5M in hexane) was added at once. The suspension has been stirred overnight. For complete lithiation the suspension was heated to 50°C and stirred for 2 more days and then filtrated and washed several times with hexane.

5.5M LiFSI: LiFSA (Nippon shokubai) and DMC (BASF) with battery grade. Electrolyte solutions were prepared by mixing the appropriate quantity of LiFSI and the solvent. The obtained electrolyte was a clear solution.

Electrochemical Measurements: Electrochemical tests were carried out in Swagelok-type cell using lithium as counter electrode. Electrode slurries were made of 90 wt. % composite and 10 wt. % polyviniylidene difluoride (PVDF) binder with N-methyl-2-pyrrolidone (NMP) as solvent. The composite consists of active material and Super C65 carbon black in a weight ratio of 80:20. The mixed slurry was coated on an aluminum foil by a doctor blade technique and dried at 120°C for 12 h under vacuum. Each working electrode (12 mm diameter) contained approximately 3 mg of active material and Li foil was used as counter electrode. LP30 from BASF (ethylene carbonate/ dimethyl carbonate, 1:1 weight ratio with 1M $LiPF_6$ was used as electrolyte. Temperature controlled galvanostatic charge-discharge experiments were conducted at 25 °C in climate chambers using an Arbin electrochemical workstation.

Electrochemical impedance spectroscopy (EIS) was performed using a three-electrode PAT-Cell (EL-CELL, Germany) with Li ring as reference electrode and Li metal (18 mm) as counter electrode. The working electrode size was 18 mm and Aluminum as the current collector. The experiments were conducted using Bio-Logic electrochemical workstation with an applied sinusoidal excitation voltage of 10 mV in the frequency range 200 kHz – 0.1Hz.

Differential electrochemical mass spectrometry: In-situ gas analysis was performed by use of differential electrochemical mass spectrometry (DEMS). The setup has been described elsewhere.[42,53] Custom cells with gas in- and outlets were assembled in an argon-filled glovebox. The cathodes used (40 mm diameter with a 4 mm hole for proper gas extraction). GF/A (42 mm diameter, GE Healthcare Life Sciences, Whatman) was used as separator, 600 µL of LP47 (1M $LiPF_6$ in ethylene carbonate/diethyl carbonate, 3:7 by weight, BASF SE) as electrolyte, and 600 µm-thick Li metal foil (Albemarle Germany GmbH) with a diameter of 40 mm as counter-electrode. A constant carrier gas flow (2.5 mL_{He}/min, purity 6.0) was applied during DEMS measurements for gas extraction. The gas was analyzed via mass spectrometry

(GSD 320, OmniStar Gas Analysis System, Pfeiffer Vacuum GmbH). After each run, a calibration gas of known composition was introduced to quantify the measured ion currents.

X-ray diffraction: Synchrotron X-ray powder diffraction (XRPD) experiments were performed at the Swiss-Norwegian Beamline (SNBL), beamline BM01, at the European Synchrotron Radiation Facility (ESRF). The powdered samples were filled in 0.5mm quartz capillaries and sealed with wax under an argon atmosphere. XRPD data were collected using a PILATUS 2M area detector from DECTRIS, a sample-to-detector distance of 142.27mm, a beam size of 0.2 x 0.2 mm, a wavelength of 0.68202Å, a 20° rotation of the capillary and an exposure time of 20s. The data were converted to conventional one-dimensional powder patterns using the FIT2D software.[54] In-house X-ray powder diffraction data were collected under rotation of the capillary on a STOE Stadi P diffractometer with Mo Kα1 (λ = 0.7093Å) using Debye-Scherrer geometry. The powder samples were sealed in quartz capillary (0.5mm in diameter) under an argon atmosphere.

Raman: Raman measurements of the surface of cycled Lithium were conducted using an ECC-Opto-Std [EL-CELL® GmbH] electrochemical cell. The washed Lithium after battery cycling was kept at the electrode side of an ECC-Opto-Std [EL-CELL® GmbH] cell and sealed with a thin optical glass window (0.15 mm) and made air-tight with a rubber seal. The whole cell was fabricated inside a Glovebox. The Raman spectra and mapping were acquired using an inVia™ confocal Raman microscope (RENISHAW) with a 532 nm laser excitation source in the spectral range 600 – 1000 cm^{-1}. A grating was used as dispersion element with a groove density of 2400 l/mm. The slit opening of the confocal system were fixed at 65 μm and centered at 1859 μm, respectively. The laser was focused on the sample using a 20× objective. The nominal laser power was filtered down to 4 mW to avoid sample overheating. Every spectrum recorded resulted from the average of 2 acquisitions of 5 s each. The data were analyzed using inVia *WiRE 4.4 Software.*

TEM:

Supporting Information

Supporting Information is available

Acknowledgements

Financial support is acknowledged by the FET-OPEN project “LiRichFCC” of the European Commission (grant agreement # 711792).

References

(1) Myung, S.-T.; Maglia, F.; Park, K.-J.; Yoon, C. S.; Lamp, P.; Kim, S.-J.; Sun, Y.-K. Nickel-Rich Layered Cathode Materials for Automotive Lithium-Ion Batteries: Achievements and Perspectives. *ACS Energy Lett.* **2017**, *2* (1), 196–223.

(2) Etacheri, V.; Marom, R.; Elazari, R.; Salitra, G.; Aurbach, D. Challenges in the Development of Advanced Li-Ion Batteries: A Review. *Energy Environ. Sci.* **2011**, *4* (9), 3243.

(3) Scrosati, B.; Hassoun, J.; Sun, Y.-K. Lithium-Ion Batteries. A Look into the Future. *Energy Environ. Sci.* **2011**, *4* (9), 3287.

(4) Koga, H.; Croguennec, L.; Menetrier, M.; Douhil, K.; Belin, S.; Bourgeois, L.; Suard, E.; Weill, F.; Delmas, C. Reversible Oxygen Participation to the Redox Processes Revealed for $Li_{1.20}Mn_{0.54}Co_{0.13}Ni_{0.13}O_2$. *J. Electrochem. Soc.* **2013**, *160* (6), 786–792.

(5) Lu, Z.; Dahn, J. R. Understanding the Anomalous Capacity of $Li/Li[Ni_xLi_{(1/3-2x/3)}Mn_{(2/3-x/3)}]O_2$ Cells Using In Situ X-Ray Diffraction and Electrochemical Studies. *J. Electrochem. Soc.* **2002**, *149* (7), 815.

(6) Rozier, P.; Tarascon, J. M. Review—Li-Rich Layered Oxide Cathodes for Next-Generation Li-Ion Batteries: Chances and Challenges. *J. Electrochem. Soc.* **2015**, *162*

(14), 2490–2499.

(7) Hy, S.; Liu, H.; Zhang, M.; Qian, D.; Hwang, B.-J.; Meng, Y. S. Performance and Design Considerations for Lithium Excess Layered Oxide Positive Electrode Materials for Lithium Ion Batteries. *Energy Environ. Sci.* **2016**, *9* (6), 1931–1954.

(8) Lee, J.; Urban, A.; Li, X.; Su, D.; Hautier, G.; Ceder, G. Unlocking the Potential of Cation-Disordered Oxides for Rechargeable Lithium Batteries. *Science (80-.).* **2014**, *343* (6170), 519–522.

(9) Yabuuchi, N.; Takeuchi, M.; Nakayama, M.; Shiiba, H.; Ogawa, M.; Nakayama, K.; Ohta, T.; Endo, D.; Ozaki, T.; Inamasu, T.; et al. High-Capacity Electrode Materials for Rechargeable Lithium Batteries: Li3NbO4 -Based System with Cation-Disordered Rocksalt Structure. *Proc. Natl. Acad. Sci.* **2015**, *112* (25), 7650–7655.

(10) Lee, J.; Seo, D.-H.; Balasubramanian, M.; Twu, N.; Li, X.; Ceder, G. A New Class of High Capacity Cation-Disordered Oxides for Rechargeable Lithium Batteries: Li–Ni–Ti–Mo Oxides. *Energy Environ. Sci.* **2015**, *8* (11), 3255–3265.

(11) Hoshino, S.; Glushenkov, A. M.; Ichikawa, S.; Ozaki, T.; Inamasu, T.; Yabuuchi, N. Reversible Three-Electron Redox Reaction of Mo 3+ /Mo 6+ for Rechargeable Lithium Batteries. *ACS Energy Lett.* **2017**, *2* (4), 733–738.

(12) Kitchaev, D. A.; Lun, Z.; Richards, W. D.; Ji, H.; Clément, R. J.; Balasubramanian, M.; Kwon, D.-H.; Dai, K.; Papp, J. K.; Lei, T.; et al. Design Principles for High Transition Metal Capacity in Disordered Rocksalt Li-Ion Cathodes. *Energy Environ. Sci.* **2018**, *11* (8), 2159–2171.

(13) KITAJOU, A.; TANAKA, K.; MIKI, H.; KOGA, H.; OKAJIMA, T.; OKADA, S. Improvement of Cathode Properties by Lithium Excess in Disordered Rocksalt Li2+2xMn1−xTi1−xO4. *Electrochemistry* **2016**, *84* (8), 597–600.

(14) Cambaz, M. A.; Vinayan, B. P.; Euchner, H.; Johnsen, R. E.; Guda, A. A.; Mazilkin, A.; Rusalev, Y. V; Trigub, A. L.; Gross, A.; Fichtner, M. Design of Nickel-Based

Cation-Disordered Rock-Salt Oxides: The Effect of Transition Metal (M = V, Ti, Zr) Substitution in LiNi 0.5 M 0.5 O 2 Binary Systems. *ACS Appl. Mater. Interfaces* **2018**, *10* (26), 21957–21964.

(15) Twu, N.; Li, X.; Urban, A.; Balasubramanian, M.; Lee, J.; Liu, L.; Ceder, G. Designing New Lithium-Excess Cathode Materials from Percolation Theory: Nanohighways in Li x Ni 2–4 x /3 Sb x /3 O 2. *Nano Lett.* **2015**, *15* (1), 596–602.

(16) Nakajima, M.; Yabuuchi, N. Lithium-Excess Cation-Disordered Rocksalt-Type Oxide with Nanoscale Phase Segregation: $Li_{1.25}Nb_{0.25}V_{0.5}O_2$. *Chem. Mater.* **2017**, *29* (16), 6927–6935.

(17) Cambaz, M. A.; Vinayan, B. P.; Clemens, O.; Munnangi, A. R.; Chakravadhanula, V. S. K.; Kübel, C.; Fichtner, M. Vanadium Oxyfluoride/Few-Layer Graphene Composite as a High-Performance Cathode Material for Lithium Batteries. *Inorg. Chem.* **2016**, *55* (8), 3789–3796.

(18) Chen, R.; Ren, S.; Knapp, M.; Wang, D.; Witter, R.; Fichtner, M.; Hahn, H. Disordered Lithium-Rich Oxyfluoride as a Stable Host for Enhanced Li + Intercalation Storage. *Adv. Energy Mater.* **2015**, *5* (9), 1401814.

(19) Ren, S.; Chen, R.; Maawad, E.; Dolotko, O.; Guda, A. A.; Shapovalov, V.; Wang, D.; Hahn, H.; Fichtner, M. Improved Voltage and Cycling for Li + Intercalation in High-Capacity Disordered Oxyfluoride Cathodes. *Adv. Sci.* **2015**, *2* (10), 1500128.

(20) Hoshino, S.; Glushenkov, A. M.; Ichikawa, S.; Ozaki, T.; Inamasu, T.; Yabuuchi, N. Reversible Three-Electron Redox Reaction of Mo 3+ /Mo 6+ for Rechargeable Lithium Batteries. *ACS Energy Lett.* **2017**, *2* (4), 733–738.

(21) Richards, W. D.; Dacek, S. T.; Kitchaev, D. A.; Ceder, G. Fluorination of Lithium-Excess Transition Metal Oxide Cathode Materials. *Adv. Energy Mater.* **2018**.

(22) Lee, J.; Papp, J. K.; Clément, R. J.; Sallis, S.; Kwon, D.-H.; Shi, T.; Yang, W.; McCloskey, B. D.; Ceder, G. Mitigating Oxygen Loss to Improve the Cycling

Performance of High Capacity Cation-Disordered Cathode Materials. *Nat. Commun.* **2017**, *8* (1), 981.

(23) Wang, X.; Huang, Y.; Ji, D.; Omenya, F.; Karki, K.; Sallis, S.; Piper, L. F. J.; Wiaderek, K. M.; Chapman, K. W.; Chernova, N. A.; et al. Structure Evolution and Thermal Stability of High-Energy- Density Li-Ion Battery Cathode Li_2VO_2F. *J. Electrochem. Soc.* **2017**.

(24) Pérez-Flores, J. C.; Villamor, R.; Ávila-Brande, D.; Gallardo Amores, J. M.; Morán, E.; Kuhn, A.; García-Alvarado, F. VO2F: A New Transition Metal Oxyfluoride with High Specific Capacity for Li Ion Batteries. *J. Mater. Chem. A* **2015**.

(25) Chen, R.; Maawad, E.; Knapp, M.; Ren, S.; Beran, P.; Witter, R.; Hempelmann, R. Lithiation-Driven Structural Transition of VO2F into Disordered Rock-Salt Li: XVO2F. *RSC Adv.* **2016**.

(26) Wang, J.; Yamada, Y.; Sodeyama, K.; Chiang, C. H.; Tateyama, Y.; Yamada, A. Superconcentrated Electrolytes for a High-Voltage Lithium-Ion Battery. *Nat. Commun.* **2016**, *7* (1), 12032.

(27) YAMADA, Y. Developing New Functionalities of Superconcentrated Electrolytes for Lithium-Ion Batteries. *Electrochemistry* **2017**, *85* (9), 559–565.

(28) Zhang, H.; Feng, W.; Nie, J.; Zhou, Z. Recent Progresses on Electrolytes of Fluorosulfonimide Anions for Improving the Performances of Rechargeable Li and Li-Ion Battery. *J. Fluor. Chem.* **2015**, *174*, 49–61.

(29) Eshetu, G. G.; Grugeon, S.; Gachot, G.; Mathiron, D.; Armand, M.; Laruelle, S. LiFSI vs. LiPF6 Electrolytes in Contact with Lithiated Graphite: Comparing Thermal Stabilities and Identification of Specific SEI-Reinforcing Additives. *Electrochim. Acta* **2013**, *102*, 133–141.

(30) Cambaz, M. A.; Vinayan, B. P.; Euchner, H.; Johnsen, R. E.; Guda, A. A.; Mazilkin, A.; Rusalev, Y. V; Trigub, A. L.; Gross, A.; Fichtner, M. Design of Nickel-Based

Cation-Disordered Rock-Salt Oxides: The Effect of Transition Metal (M = V, Ti, Zr) Substitution in LiNi0.5M0.5O2 Binary Systems. *ACS Appl. Mater. Interfaces* **2018**, *10* (26), 21957–21964.

(31) Cambaz, M. A.; Vinayan, B. P.; Clemens, O.; Munnangi, A. R.; Chakravadhanula, V. S. K.; Kübel, C.; Fichtner, M. Vanadium Oxyfluoride/Few-Layer Graphene Composite as a High-Performance Cathode Material for Lithium Batteries. *Inorg. Chem.* **2016**, *55* (8), 3789–3796.

(32) Momma, K.; Izumi, F. VESTA 3 for Three-Dimensional Visualization of Crystal, Volumetric and Morphology Data. *J. Appl. Crystallogr.* **2011**, *44* (6), 1272–1276.

(33) Aurbach, D.; Markovsky, B.; Salitra, G.; Markevich, E.; Talyossef, Y.; Koltypin, M.; Nazar, L.; Ellis, B.; Kovacheva, D. Review on Electrode–electrolyte Solution Interactions, Related to Cathode Materials for Li-Ion Batteries. *J. Power Sources* **2007**, *165* (2), 491–499.

(34) Wang, J.; Yamada, Y.; Sodeyama, K.; Chiang, C. H.; Tateyama, Y.; Yamada, A. Superconcentrated Electrolytes for a High-Voltage Lithium-Ion Battery. *Nat. Commun.* **2016**, *7* (1), 12032.

(35) Biesinger, M. C.; Lau, L. W. M.; Gerson, A. R.; Smart, R. S. C. Resolving Surface Chemical States in XPS Analysis of First Row Transition Metals, Oxides and Hydroxides: Sc, Ti, V, Cu and Zn. *Appl. Surf. Sci.* **2010**, *257* (3), 887–898.

(36) Lee, S.-H.; Cheong, H. M.; Je Seong, M.; Liu, P.; Tracy, C. E.; Mascarenhas, A.; Pitts, J. R.; Deb, S. K. Microstructure Study of Amorphous Vanadium Oxide Thin Films Using Raman Spectroscopy. *J. Appl. Phys.* **2002**, *92* (4), 1893–1897.

(37) Zhang, C.; Yang, Q.; Koughia, C.; Ye, F.; Sanayei, M.; Wen, S.-J.; Kasap, S. Characterization of Vanadium Oxide Thin Films with Different Stoichiometry Using Raman Spectroscopy. *Thin Solid Films* **2016**, *620*, 64–69.

(38) Yamamoto, T. Assignment of Pre-Edge Peaks in K-Edge x-Ray Absorption Spectra of

3d Transition Metal Compounds: Electric Dipole or Quadrupole? *X-Ray Spectrom.* **2008**, *37* (6), 572–584.

(39) Twu, N.; Metzger, M.; Balasubramanian, M.; Marino, C.; Li, X.; Chen, H.; Gasteiger, H.; Ceder, G. Understanding the Origins of Higher Capacities at Faster Rates in Lithium-Excess $Li_xNi_{2-4x/3}Sb_{x/3}O_2$. *Chem. Mater.* **2017**, *29* (6), 2584–2593.

(40) Strehle, B.; Kleiner, K.; Jung, R.; Chesneau, F.; Mendez, M.; Hubert, A. The Role of Oxygen Release from Li- and Mn-Rich Layered Oxides During the First Cycles Investigated by On-Line Electrochemical Mass Spectrometry. *J. Electrochem. Soc.* **2017**, *164* (2), 400–406.

(41) Metzger, M.; Strehle, B.; Solchenbach, S.; Gasteiger, H. A. Origin of H2 Evolution in LIBs: H2O Reduction vs. Electrolyte Oxidation. *J. Electrochem. Soc.* **2016**, *163* (5), A798–A809.

(42) Berkes, B. B.; Schiele, A.; Sommer, H.; Brezesinski, T.; Janek, J. On the Gassing Behavior of Lithium-Ion Batteries with NCM523 Cathodes. *J. Solid State Electrochem.* **2016**, *20* (11), 2961–2967.

(43) Metzger, M.; Sicklinger, J.; Haering, D.; Kavakli, C.; Stinner, C.; Marino, C.; Gasteiger, H. A. Carbon Coating Stability on High-Voltage Cathode Materials in H 2 O-Free and H 2 O-Containing Electrolyte. *J. Electrochem. Soc.* **2015**, *162* (7), A1227–A1235.

(44) Cabana, J.; Kwon, B. J.; Hu, L. Mechanisms of Degradation and Strategies for the Stabilization of Cathode–Electrolyte Interfaces in Li-Ion Batteries. *Acc. Chem. Res.* **2018**, *51* (2), 299–308.

(45) Vetter, J.; Novák, P.; Wagner, M.; Veit, C.; Möller, K.-C.; Besenhard, J. O.; Winter, M.; Wohlfahrt-Mehrens, M.; Vogler, C.; Hammouche, A. Ageing Mechanisms in Lithium-Ion Batteries. *J. Power Sources* **2005**, *147* (1–2), 269–281.

(46) Assat, G.; Tarascon, J.-M. Fundamental Understanding and Practical Challenges of

Anionic Redox Activity in Li-Ion Batteries. *Nat. Energy* **2018**, *3* (5), 373–386.

(47) Li, L.; Zhou, S.; Han, H.; Li, H.; Nie, J.; Armand, M.; Zhou, Z.; Huang, X. Transport and Electrochemical Properties and Spectral Features of Non-Aqueous Electrolytes Containing LiFSI in Linear Carbonate Solvents. *J. Electrochem. Soc.* **2011**, *158* (2), A74.

(48) Qian, J.; Henderson, W. A.; Xu, W.; Bhattacharya, P.; Engelhard, M.; Borodin, O.; Zhang, J.-G. High Rate and Stable Cycling of Lithium Metal Anode. *Nat. Commun.* **2015**, *6* (1), 6362.

(49) Golden, J. H.; DiSalvo, F. J.; Frechet, J. M. J. Room-Temperature Synthesis of (LiMo3Se3)n and the Determination of the Relative Reduction Potential of Tert-Butyllithium. *Chem. Mater.* **1994**, *6* (6), 844–849.

(50) Yabuuchi, N.; Nakayama, M.; Takeuchi, M.; Komaba, S.; Hashimoto, Y.; Mukai, T.; Shiiba, H.; Sato, K.; Kobayashi, Y.; Nakao, A.; et al. Origin of Stabilization and Destabilization in Solid-State Redox Reaction of Oxide Ions for Lithium-Ion Batteries. *Nat. Commun.* **2016**, *7* (1), 13814.

(51) Chen, R.; Ren, S.; Yavuz, M.; Guda, A. A.; Shapovalov, V.; Witter, R.; Fichtner, M.; Hahn, H. Li+ Intercalation in Isostructural Li2VO3 and Li2VO2F with O2- and Mixed O2-/F- Anions. *Phys. Chem. Chem. Phys.* **2015**, *17* (26), 17288–17295.

(52) Abdellahi, A.; Urban, A.; Dacek, S.; Ceder, G. Understanding the Effect of Cation Disorder on the Voltage Profile of Lithium Transition-Metal Oxides. *Chem. Mater.* **2016**, *28* (15), 5373–5383.

(53) Berkes, B. B.; Jozwiuk, A.; Vračar, M.; Sommer, H.; Brezesinski, T.; Janek, J. Online Continuous Flow Differential Electrochemical Mass Spectrometry with a Realistic Battery Setup for High-Precision, Long- Term Cycling Tests. *Anal. Chem.* **2015**, *87* (12), 5878 − 5883.

(54) Hammersley, A. P.; Svensson, S. O.; Hanfland, M.; Fitch, A. N.; Hausermann, D. Two-

Dimensional Detector Software: From Real Detector to Idealised Image or Two-Theta Scan. *High Press. Res.* **1996**, *14* (4–6), 235–248.